Collision-Induced Fine-Structure Transitions of $Hg(6^3P_1 \rightarrow 6^3P_0)$ with N_2 and CO. 1. Initial Orbital Alignment Effects

Misaki Okunishi,* Junichi Hashimoto, Hisashi Chiba, Kenji Ohmori, Kiyoshi Ueda, and Yukinori Sato

Research Institute for Scientific Measurements, Tohoku University, Katahira, Sendai, 980-8577, Japan

Received: October 26, 1998; In Final Form: January 13, 1999

Effects of initial orbital alignment have been investigated for the fine-structure transitions of $Hg(6^3P_1 \rightarrow 6^3P_0)$ induced by collisions with N_2 and CO in a crossed molecular beam experiment using a laser pump−probe technique. The orbital alignment effects are observed by monitoring the population of the product $Hg(6^3P_0)$ as a function of polarization angle (θ) of the linearly polarized pump laser, which prepares the $Hg(6^3P_1)$, relative to the direction of the initial relative velocity vector. The alignment effects in this study are represented by an asymmetry parameter β in the angle-dependent cross section, $\sigma(\theta) = \sigma_0[1 + \beta P_2(\cos\theta)]$. The measurement for $Hg-N_2$ exhibits a large alignment effect with $\beta = -0.50(7)$, but for Hg−CO a small effect with $\beta = -0.20(6)$. Both processes show preference for perpendicular excitation of the pump laser with $\theta = 90°$. The nonadiabatic transitions responsible for this fine-structure process therefore occur mainly via the $\tilde{B}(2^3A' + 2^3A'')$ molecular electronic state and not via the $\tilde{A}(1^3A')$ state for $Hg-N_2$. In contrast, the small effect for Hg−CO indicates that the contribution from the nonadiabatic transition via the $\tilde{A}$ state is comparable with that via the $\tilde{B}$ state for Hg−CO.

I. Introduction

Mercury atoms are excited to a 6^3P_1 state from the ground state (6^1S_0) through photoabsorption of 253.7 nm light and then usually decay by emitting fluorescence of the same wavelength with a lifetime of 114 ns.[1] However, when they collide with molecules, the fluorescence from the excited state is quenched through chemical reactions or inelastic energy transfers. Collisional inelastic and reactive processes initiated by the photoabsorption of mercury are called mercury photosensitized processes and have been the subjects of many experimental studies for a long time.[2−7] Among them, the target of the present study is intramultiplet transitions of $Hg(6^3P_1-6^3P_0)$ induced by collisions with molecules(M),

$$Hg(6^3P_1) + M \rightarrow Hg(6^3P_0) + M^{\#} \times (\Delta E(^3P_1-^3P_0) = 1767\ cm^{-1}) \quad (1)$$

which is an important elementary process in mercury photosensitized reactions, because it produces a metastable state of $Hg(6^3P_0)$ with a considerable amount of internal energy (E = 37645 cm^{-1}) which leads to subsequent chemical reactions.[2−6]

When the collision partners are rare gases, no quenching processes are observed but collisions with molecules lead to these quenching processes efficiently. Accordingly, internal motions of the molecules and anisotropy of electrostatic interactions between the Hg and molecules are expected to be of great importance in these inelastic quenching processes. We selected two diatomic molecules, N_2 and CO, as the collision partners in the present study because they are isoelectronic molecules with the same mass number and similar polarizability, but the cross section for CO (σ = 22 Å^2) is about 30 times larger than that for N_2 (σ = 0.77 Å^2).[7] Furthermore, since total quenching cross sections are almost the same as the partial cross sections for the fine-structure transitions of the $Hg-N_2$ and Hg−CO systems,[7] this fine-structure changing process is the main pathway in the collisional quenching of $Hg(6^3P_1)$ with both N_2 and CO.

To understand the mechanism of them in detail, we have to know (i) which electronic surface is more efficient for this inelastic process, (ii) where the nonadiabatic transition responsible for process 1 is localized in the potential surface, and so on. The main subject of the present manuscript is related to the feature (i) by observing effects of an atomic orbital alignment of the excited $Hg(6^3P_1)$ on the relative cross sections for the fine-structure process (1) with M = N_2 and CO. In the following article (referred to as paper 2 in this manuscript), we describe the translational energy dependence of the cross sections to discuss the problem (ii).[8]

Figure 1 shows schematically the intermolecular potentials of an $Hg-AB(^1\Sigma^+)$ (AB = diatomic molecule) relevant to the present fine-structure process. Three electronic states can be responsible for process (1) as initial molecular states, which correlate with the $Hg(6^3P_1)$ at an infinite nuclear separation. Two ($2^3A'$ and $2^3A''$) of them are degenerate in a linear configuration and denoted as the $\tilde{B}$ state, and the last one ($1^3A'$) is the $\tilde{A}$ state, just like the potential curves of Hg−rare gas systems.[9,10] The electronic state correlating with the product $Hg(6^3P_0)$ is the $\tilde{a}$ ($1^3A''$) state. The purpose of this experiment is to obtain information on molecular state selectivity between the $\tilde{A}$ and $\tilde{B}$ states in the fine-structure process (1) with N_2 and CO. The state selectivity in collisions of excited atoms with rare gases or closed-shell molecules are described as orbital alignment effects of the excited atoms in lots of problems in low-energy atomic collisions.[11−52] There are two kinds of experimental methods to elucidate the effects of initial orbital alignment of the excited atoms, i.e., (i) precollision alignment method[11−28] and (ii) half-collision alignment method.[29−52] The

* Corresponding author. E-mail: okunishi@rism.tohoku.ac.jp.

10.1021/jp9841844 CCC: $18.00
Published on Web 03/09/1999

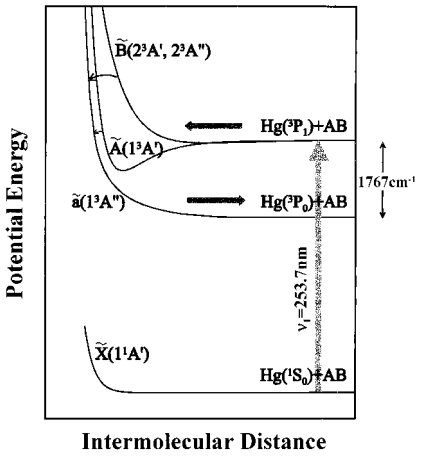

Figure 1. Schematic potential energy diagram of the Hg−AB (AB = diatomic molecule) system relevant to the present fine-structure transitions and the ground electronic state. The B̃ state consists of two molecular electronic states, $2^3A'$ and $2^3A''$.

half-collision method has already been applied to the present fine-structure process with N_2 and CO,[30,31,51] and in the present study, we have employed the precollision alignment method to reveal the alignment effect of the atomic orbital of $Hg(6^3P_1)$. We summarize, here, these methods and their applications to the present fine-structure process in the half-collision experiments as follows.

(i) Precollision alignment method, where alignment of an excited atomic orbital is achieved prior to the collision by polarized laser radiation under crossed-beam or beam-gas conditions. The effects of the orbital alignment are measured as a function of the polarization angle of the laser radiation with respect to the initial relative velocity of approach (collision velocity). In this kind of experiment, one can obtain only partial state selectivity of the molecular states because the molecular axis is defined in the molecule-fixed frame and does not coincide with the initial collision velocity, which is referenced to the space-fixed frame. This is, however, a universal technique with less restriction of the target species and has been widely applied to a variety of collisional events such as electronic deexcitation and excitation energy transfers,[13−15] electronic-to-vibrational energy transfers,[16−18] near-resonant energy transfers,[19−22] intramultiplet mixings,[23−25] and chemical reactions.[26−28]

(ii) Half-collision alignment method, where a binary collision complex is optically pumped to an excited molecular state to initiate inelastic or reactive collision processes. The selection of a molecular state is achieved by the choice of an excitation wavelength around the corresponding atomic transition, and therefore, the state selectivity is usually fairly good unless more than two electronic states are simultaneously excited accidentally.

There are two types of situations in the half-collision experiments. In one situation, bound states of stabilized van der Waals (vdW) molecules in supersonic free jets are used as initial states for the photoexcitations,[29−38] and in another one, free states of transient collision complex are used under thermal energy conditions in gas cell experiments.[39−52] Spectroscopic studies on intramultiplet predissociations of the $Hg(6^3P_1)-N_2$ and $Hg(6^3P_1)-CO$ vdW molecules to $Hg(6^3P_0) + N_2$ and CO have already been reported.[30,31] These studies have shown that the predissociation rate of $Hg-N_2$ in the Ã state depends on rotational and vibrational quantum numbers and conclude that the overall rotation of the complex and the bending motion (i.e., restricted internal rotation) of N_2 accelerate the predissociation rate. In addition, the average predissociation rates were almost in the same order for both the Ã and B̃ states. For Hg−CO, no detailed information was obtained because the predissociation rate was too fast to observe well-resolved vibronic structures. Although this method is useful to study the photodissociation of the vdW complex in a state-to-state sense, the dynamical conditions are far from those in the full collision processes; for example, the initial collision velocity and the range of angular momentum (l) associated with the relative nuclear motion are completely different.

The excitation of the collision complex in the latter situation was accomplished via an optical collision process, in which absorption of light occurs during the collision.[39−52] The selection of the molecular state was achieved by photoabsorption in (far) red or blue wings of a collisionally broadened atomic transition, which usually lead to the excitation to the different molecular electronic states. We have recently applied a laser pump and probe technique in the far-wing spectral region of the Hg atomic resonance line ($6^3P_1-6^1S_0$) broadened by collisions with N_2 and CO to study the fine-structure process (1).[51] The dynamical conditions in these experiments are almost the same as those in the full collision processes. It is, therefore, possible to obtain information on the molecular state selectivity under the full-collision conditions from the analysis of the broad far-wing excitation spectrum. For $Hg-N_2$, we found that this fine-structure process took place mainly via the B̃ state and the contribution of the nonadiabatic transition via the Ã state was negligibly small. The intermolecular potentials of $Hg-N_2$, which are indispensable for the correct analysis of the far-wing excitation spectrum to separate the free−free and bound−free components in the spectrum, had been known with a considerable accuracy from the photoexcitation studies of the $Hg-N_2$ vdW molecule[30,31] as well as the analysis of the far-wing absorption spectrum.[51] On the other hand, since almost no information was available on the intermolecular potentials for Hg−CO, it was impossible to know its state selectivity. Furthermore, the measurement of the far-wing absorption spectrum of Hg−CO, which is also indispensable for the analysis of the far-wing excitation spectrum, could not be observed due to its experimental difficulty.

In the present experiment, we employed the precollision alignment method under crossed molecular beam conditions to investigate the orbital alignment effects of the excited $Hg(6^3P_1)$ for the fine-structure transitions (1) with N_2 and CO. Despite measuring integral cross sections, we observed a large alignment effect for $Hg-N_2$, with a preference for perpendicular alignment with respect to the initial collision velocity. These results clearly indicate a preference of the B̃ state for this fine-structure transition, as expected from our previous far-wing experiment.[51] In contrast, a small effect was observed for Hg−CO, and it also favors the perpendicular alignment. This means that the contribution of the nonadiabatic transition from the Ã state is not negligible for Hg−CO. The difference between the results of $Hg-N_2$ and Hg−CO is readily explained by anisotropy of electrostatic interactions between the $Hg(6^3P_J)$ and diatomic molecules (N_2 and CO) at shorter internuclear separations.

II. Experimental Section

A. Crossed Molecular Beam Apparatus. All experiments in this study were carried out in a crossed molecular beam apparatus schematically illustrated in Figure 2, which consists of two differentially pumped source chambers of pulsed molecular beams, a main scattering chamber, and a detection system of laser-induced fluorescence (LIF).

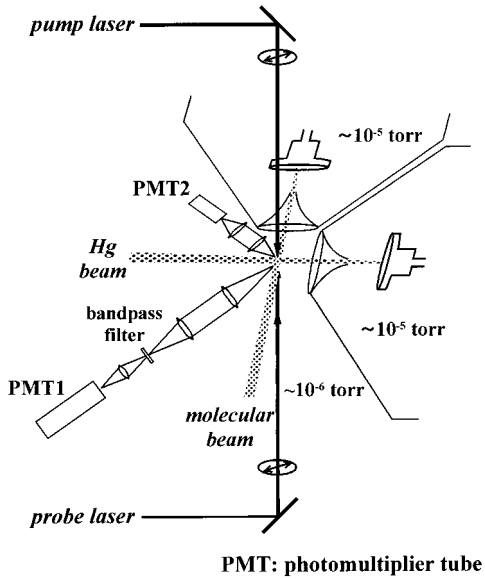

Figure 2. Schematic drawing of the apparatus for the crossed molecular beam experiment.

A mercury beam was crossed with a molecular beam of N_2 or CO perpendicularly at the scattering center of the main chamber, which was evacuated by a 6 in. diffusion pump with a liquid-nitrogen baffle. A liquid-nitrogen trap was also located in the main chamber to trap the mercury atoms from the first source chamber of the Hg beam. This configuration enabled the operating pressure to be maintained in the low 10^{-6} Torr range and the base pressure about 1.5×10^{-7} Torr.

The pulsed supersonic beam of Hg seeded in helium gas was generated with a pulsed valve (General Valve 9-Series, 0.4 mm orifice) operated at 10 Hz in one source chamber. The valve was equipped with an mercury reservoir heated to 200 °C to obtain enough vapor pressure (15 Torr). The stagnation pressure of the carrier gas (He) was kept at 2 atm. The Hg beam was collimated with a nickel skimmer (Beam Dynamics, 1.5 mm orifice) and introduced into the scattering center of the main chamber, 55 mm downstream from the nozzle orifice of the Hg valve. The skimmer was 15 mm away from the nozzle orifice to make the diameter of the beam about 5.5 mm at the scattering center. The velocity of the Hg was determined to be 1790 m/sec at the scattering region by a time-of-flight measurement, which is described in detail in paper 2. This Hg source chamber was evacuated by a 10 in. diffusion pump with a liquid-nitrogen trap, and the pressure was maintained in the low 10^{-5} Torr range during operation.

The supersonic molecular beam of pure N_2 (Nippon Sanso, purity >99.9999%) or CO (Nippon Sanso, purity >99.95%) without seeding gas was produced with a second pulsed valve (General Valve 9-Series, 0.8 mm orifice) in another source chamber, and the valve was operated at 5 Hz for shot-by-shot subtraction of background signals. The molecular beam passed through a nickel skimmer (Beam Dynamics, 2.0 mm orifice) and a homemade stainless aperture with a 3 mm orifice into the main chamber, and the beam diameter was about 5 mm at the scattering center. The total distance to the nozzle orifice of the second valve from the scattering center was also 55 mm. The velocity of the N_2 or CO beam was estimated to be 770 m/sec.[8] The rotational temperature of the CO in the molecular beam was observed to be about 15 K under the present experimental condition by a measurement of a rotationally resolved (2 + 1) resonantly enhanced multiphoton ionization spectra of the $E^1\Pi-X^1\Sigma^+$ (0,0) band of CO.[53,54] Since N_2 has similar properties to CO as a gas, such as mass number, viscosity, polarizability, and so on, we assume that the rotational temperature of N_2 is about the same as that of CO under the same operating condition. This second source chamber was evacuated by a 6 in. diffusion pump, and the pressure was kept at about 1×10^{-5} Torr during the operation.

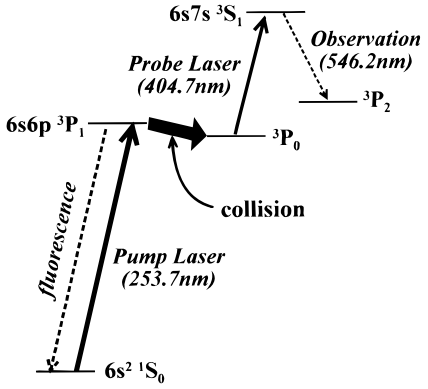

Figure 3. Energy diagram of mercury illustrating the excitation and detection schemes, with their transition wavelengths.

B. Preparation of the Aligned Hg(6^3P_1) and Probe of the Metastable Hg(6^3P_0). Figure 3 shows an energy diagram of the Hg atom relevant to the present experiment with their transition wavelengths. The Hg atom at the interaction region was excited to the 6^3P_1 state by linearly polarized laser light at 253.7 nm (pump laser), which was obtained by frequency doubling the output of a pulsed dye laser (Spectra Physics PDL-2) pumped by the 355 nm output of a Nd:YAG laser (Spectra Physics GCR 130). A second dye laser (PDL-2) was excited by the 532 nm output of another Nd:YAG laser (Spectra Physics DCR-3). The probe laser light at 404.7 nm was generated by frequency mixing of the output of the second dye laser and the fundamental output (1064 nm) of the Nd:YAG laser, in which an intracavity Etalon was inserted. The two laser beams passed through light baffles into the interaction region in the main chamber collinearly and intersected both the Hg and molecular beams at right angles.

A spacial filter with a 200 mm pinhole was used to obtain a uniform beam of the pump laser, which was necessary to prepare the Hg(6^3P_1) without saturation of the atomic transition. We confirmed this by measuring the power dependence of the resonance fluorescence at 253.7 nm before starting each experiment. The polarization of the pump laser pulse was improved by a Gran laser prism and its direction was rotated by a double Fresnel rhomb polarization rotator. The polarization purity of the pump laser was estimated to be >95%.

Fluorescence Hg($7^3S_1 \rightarrow 6^3P_2$) was detected with a photomultiplier tube (Hamamatsu R374, PMT1 in Figure 2) through a bandpath filter centered at 546.2 nm and a notch filter which reflected light only around 253.7 nm, as a function of the polarization angle of the pump laser. The measurements were performed with an interval of 20°, and the order of the measurements were determined randomly to avoid systematic errors. The fluorescence at 253.7 nm was detected simultaneously with another photomultiplier tube (Hamamatsu R1464, PMT2 in Figure 2) to normalize the probe signal with the PMT1, because this signal is proportional to the amount of the Hg(6^3P_1) at the interaction region and can be used to correct the fluctuation of power of the pump laser light as well as the density of the ground-state Hg in the atomic beam. The signals obtained with the PMT1 and PMT2 were amplified and integrated by boxcar integrators (SRS SR250) for 400 laser shots

per angle in each run. The fluorescence from Hg(6^3P_1) measured with the PMT2 also depended on the polarization angle of the pump laser and this dependence was not related to the amount of the Hg(6^3P_1). Hence, we measured this polarization angle dependence in each experiment to correct the normalization procedure of the probe signal.

If an excited atom has a hyperfine structure caused by a coupling with its nuclear spin, this hyperfine coupling makes the problem more complicated and usually reduces the polarization dependence significantly.[13] There are six main isotope species in Hg, and two of them (^{199}Hg and ^{201}Hg) have odd mass numbers with nonzero nuclear spin moments. The natural abundances of ^{199}Hg and ^{201}Hg are 16.9% and 13.2%, respectively. The resolution of our lasers ($\sim$0.5 cm^{-1}) is not high enough to separate these isotope and hyperfine splittings of the two atomic transitions. However, the atomic line ($7^3S_1-6^3P_0$) at 404.7 nm has large hyperfine splittings (0.3−0.7 cm^{-1}) for odd mass species but small isotope splittings (less than 0.1 cm^{-1}) for even mass species, which have no hyperfine structures.[55] Thus, we estimated that the contribution from the even number species to the total absorption was more than 90% when the probe laser frequency was tuned to the center of the atomic line ($7^3S_1-6^3P_0$).

Since the 6^3P_1 state of mercury has a large g factor (g = 1.479),[56] the electronic angular momentum (J) is likely to precess around the direction of the magnetic field at the interaction region, which is induced by the earth's field and the solenoids of the two pulsed valves. To estimate the effect of the residual magnetic field on our measurements we observed the polarization dependence with several delay times between the pump and probe lasers and found that delay times less than 50 ns were sufficiently short to avoid this effect within our experimental errors. The precession time was estimated by the frequency of the Zeeman quantum beat observed in the resonance fluorescence of the atomic transition ($6^3P_1-6^1S_0$) and was about 300−400 ns under the present experimental condition. Therefore, all measurements of the polarization dependence in this study were carried out with the delay time of 50 ns.

III. Results and Discussion

A. Evolution of the Electronic Orbital of the Excited Hg(6^3P_1). To understand the effect of the initial orbital alignment in the present experiment, we must describe the evolution of the atomic orbital of the excited Hg(6^3P_1) during the collision. This is accomplished by classifying the molecular electronic states using Hund's coupling schemes as a function of the internuclear separation, as depicted in Figure 4, because the molecular electronic state of the colliding pair may be adequately described by one of the Hund's coupling schemes at each stage of the collision.[57] The triplet character of the excited state of Hg(6^3P_1) results in a more complicated situation than a singlet state, due to the existence of the nonzero spin angular momentum (S = 1). When linearly polarized laser light excites a mercury atom in its ground state to the 6^3P_1 state, the total electronic orbital (including spin) of Hg(6^3P_1) is aligned parallel to the direction of the laser polarization in the space-fixed frame. The charge cloud of the 6p electron coming from the Hg(6^3P_1) state is therefore proportional to $|Y_{11}(\theta,\phi)|^2$ distribution as shown schematically in Figure 4c, where θ and ϕ are polar angles of the 6p electron with respect to the electric field vector $\mathbf{E}_{las}$, and $Y_{11}(\theta,\phi)$ is a spherical harmonic function (see Appendix). Thus, we use the concept of "orbital alignment" to express this angular property of the electronic wave function of the excited Hg atom.

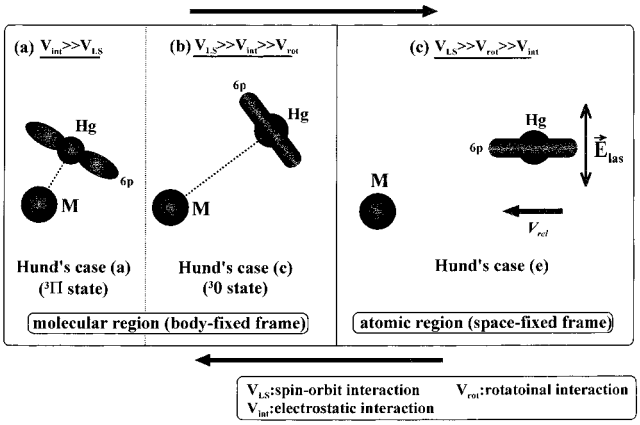

Figure 4. Evolution of the atomic orbital of Hg(6^3P_1) during the collision depicted schematically. It is classified using Hund's coupling schemes at each stage of the collision.

If there is no external electric or magnetic field, the atomic orbital retains its alignment before spontaneous emission. However, when it collides with a molecule, the direction of the atomic orbital varies during the collision. At large internuclear separations where the electrostatic interaction (V_{int}) between the Hg and molecule (M) is much less than the rotational coupling (V_{rot}) with respect to the relative nuclear motion, the direction of the atomic orbital is space fixed and its direction remains unchanged, as shown in Figure 4c. On the other hand, in molecular regions ($V_{int}(R) \gg V_{rot}(R)$) where the atomic orbital is fixed to the molecular axis of this system, the atomic orbital rotates as the molecular axis rotates during the collision.[11] How the atomic orbital is fixed to the molecular axis is called as an "orbital locking process" and it plays an essential part in understanding the orbital alignment effect.[11−15,58,59]

There are two ways to couple the atomic orbital to the molecular axis, depending on the relative strength of the electrostatic interaction (V_{int}) to the spin−orbit interaction (V_{LS}). In the region where $V_{LS}(R) \gg V_{int}(R)$ at relatively large internuclear separations, the atomic orbital including spin is fixed to the molecular axis and the molecular states in this region are classified by the projection (Ω) of the total angular momentum (J) onto the molecular axis, as shown in Figure 4b (Hund's case (c)). At much shorter internuclear separations where $V_{LS}(R) \ll V_{int}(R)$, the atomic orbital without spin, the 6p orbital of Hg here, is coupled to the molecular axis and the character of the molecular state is described by the projection (Λ) of the total electronic angular momentum (L) without spin, as depicted in Figure 4a (Hund's case (a) or case (b)). Therefore, we have to consider the transformation of the character of molecular states from case (c) to case (a) at an intermediate region where $V_{int}(R) \approx V_{LS}(R)$, and this change of the electronic character of molecular states often causes the nonadiabatic transitions between the different molecular states.[57] In the present situation, however, the molecular electronic states are well characterized by the Hund's case (c) wave functions in a wide range of intermolecular separations due to a large spin−orbit interaction of Hg(6^3P_J), where the spin−orbit constant is about 2100 cm^{-1}. Thus, we only have to consider how the atomic orbital characterized by $|J, M_J\rangle$ in the space-fixed frame, where M_J is the projection of J onto the space-fixed axis, is locked to the molecular axis in the intermediate region where $V_{int}(R) \approx V_{rot}(R)$ here.

In addition to the orbital locking to the molecular axis, we have to consider how the atomic orbital is locked to the *molecular plane* (system plane) which contains the three nuclei

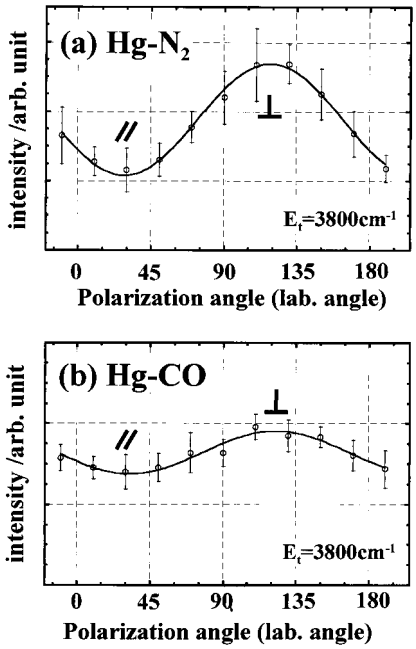

Figure 5. Results of the polarization angle dependence of the pump laser on the relative cross sections by collisions with (a) N_2 and (b) CO, normalized by the LIF intensity from $Hg(6^3P_1)$ at 253.7 nm. The solid lines are the results of least-squares fitting to eq 2. Parallel (∥) and perpendicular (⊥) in the figures mean that the direction of the polarization is parallel and perpendicular to the direction of the initial collision velocity vector.

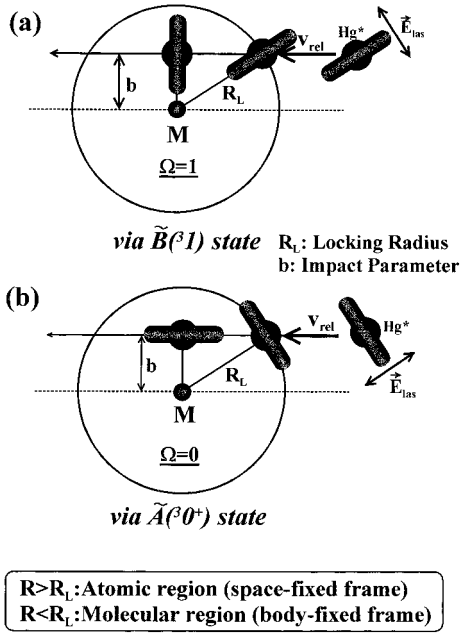

Figure 6. Schematic view of the orbital locking motion of $Hg(6^3P_1)$ to the (a) Ã or (b) B̃ molecular state.

in the atom−diatom collisions. We can describe this locking process in the same way as is done for the orbital locking to the molecular axis.[17] At relatively large internuclear separations, the energy separation of the A′ and A″ components of the B̃ state is much less than the rotational energies associated with the out-of-plane rotation of the diatomic molecule. In this region, the reflection symmetry with regard to the *collision plane*, which contains the colliding pair and its relative collision velocity, is almost conserved in the space-fixed frame just like in atom−atom collisions. At much shorter internuclear separations, anisotropy of the electrostatic interaction between the Hg and diatomic molecule is large and reflection symmetry with regard to the *molecular plane* is almost conserved in the molecular-fixed frame.

B. Results of the Polarization Dependence Measurements. Relative cross sections for the fine-structure transitions in the Hg−N_2 and Hg−CO collisions are shown in parts a and b of Figure 5 as a function of the laboratory polarization angle (θ_{lab}) of the linearly polarized pump laser. Both of the measurements were carried out with relative translational energy of 3800 cm^{-1}. Since the product state (6^3P_0) of Hg has no alignment ($J = 0$), we do not need to worry about the direction of the probe laser polarization. The symbols "perpendicular" and "parallel" in these figures mean that the direction of the pump laser polarization is perpendicular and parallel to the initial collision velocity, respectively. The origin of the laboratory angle is defined to be almost parallel to the direction of the Hg atomic beam. The solid lines are results of the least-squares fitting using a function[60]

$$\sigma(\theta_{lab}) = \sigma_0[1 + \beta P_2(\cos(\theta_{lab} - \theta_0)] \qquad (2)$$

where $P_2(\cos(\theta))$ is the second-order Legendre polynomial and β is the asymmetry parameter. As seen in Figure 5, we obtained a large polarization effect for Hg−N_2 but a small effect for Hg−CO. Both of them also show a preference for perpendicular excitation of the pump laser.

To obtain a simple picture on the polarization dependence in this experiment, we use an "orbital locking and following model", in which the atomic orbital is suddenly locked to the molecular axis at an adequate internuclear separation (R_L), called as a "locking radius". This model has been widely used to describe the inelastic collisions of the polarized atoms[11−15,17,19,20,22,24−25] or the collisional redistribution of radiation in optical collisions.[44−46] Assuming a straight-line trajectory with an impact parameter *b*, Figure 6 illustrates the evolution of the atomic orbital of the $Hg(6^3P_1)$ in this approximation. Figure 6a shows the orbital locking process with the formation of the "+" component of the $\tilde{B}(^31)$ molecular state and Figure 6b shows the formation of the $\tilde{A}(^30^+)$ state. The orbital locking motion is located at relatively large internuclear separations where the anisotropy of the electrostatic interaction is small, and therefore, atom−atom notation is used to describe the molecular states.

Since the nonadiabatic transitions from the Ã and/or B̃ states to the ã state are expected to occur at small distances *R* (as discussed in paper 2), the range of impact parameter involved in the present fine-structure process must be much smaller than the R_L. Hence, when the laser polarization is perpendicular to the initial collision velocity, most of the trajectories with this perpendicular alignment are connected to a molecular state with $\Omega = 1$, which is the $B(^31)$ state here, as shown in Figure 6a. On the other hand, parallel excitation with respect to the collision velocity is mainly related to a molecular state with $\Omega = 0$ ($A(^30^+)$ state) as shown in Figure 6b. The present picture is, of course, too simple, because we observe only integral cross sections averaged over the impact parameter *b* (and azimuthal angle), and therefore, perfect selection of the molecular state cannot actually be achieved. However, the large polarization effect for Hg−N_2 in our experiment clearly indicates that the main route for the present inelastic process is that via the B̃ state. On the other hand, there must be a considerable contribution from nonadiabatic transitions via the Ã state for Hg−CO.

The contribution of the nonadiabatic transition via the Ã state relative to that via the B̃ state for Hg−CO is estimated roughly

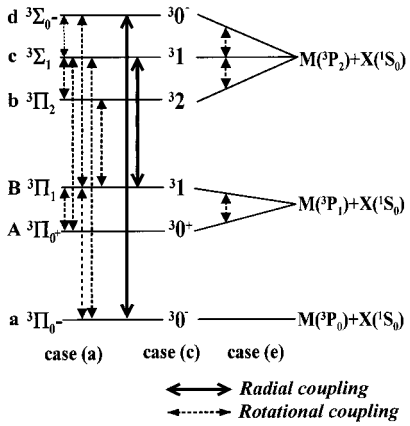

Figure 7. Nonadiabatic couplings responsible for the intramultiplet mixing of M(*ns*n*p* ^3P_J) sublevels in atom−atom collisions in each Hund's case region.

as 0.7, using the polarization dependence for Hg−N_2 as a standard. In this estimation, we tried to reproduce the shape of the polarization dependence for Hg−CO in Figure 5b by adding the polarization dependence for Hg−N_2 in Figure 5a and a hypothetical flat dependence ($\beta = 0$) with an appropriate ratio, from which we could calculate the relative contribution from the $\tilde{A}$ state for Hg−CO. In this calculation, we assume that the polarization dependence for the limiting case when the contribution from the $\tilde{A}$ state is negligible would be given by the curve for Hg−N_2 in Figure 5a and that the polarization dependence should be flat when the nonadiabatic transitions via the $\tilde{A}$ and $\tilde{B}$ states contribute equally to this fine-structure process. This simple estimation neglects details of the differences in the potentials between the Hg−N_2 and Hg−CO systems. However, it may be assumed that the locking radii of the two systems are not so different, because the intermolecular potentials for Hg−N_2 and Hg−CO should be similar at large internuclear separations due to the similar values of the polarizability for N_2 and CO ($\alpha = 17.6$ and 19.5×10^{25} cm^3, respectively[61]). The present estimation also neglects the differences in the shape of opacity functions between these two systems. In low-energy collisions, the range of impact parameters involved in nonadiabatic transitions usually changes rapidly as a function of the collision energy; for example, as shown in paper 2, the cross sections for Hg−N_2 show energy threshold for appearance of the Hg(6^3P_0) at a collision energy around 900 cm^{-1}, where only collisions with very small impact parameters lead to the nonadiabatic transition and a large polarization dependence with $\beta \approx -1$ is expected. Hence, direct comparison of the polarization dependence for the different species is difficult at such low collision energies. However, the cross sections show almost flat energy dependence around the present collision energy ($E_t \approx$ 3800 cm^{-1}) in both Hg−N_2 and Hg−CO collisions (see paper 2), and therefore, the direct comparison of the polarization dependences for these two systems is possible, approximately. We can thus claim for Hg−CO that the transition probability from the $\tilde{A}$ state is a little less than that from the $\tilde{B}$ state but of the same order.

C. Discussion of the Mechanism for the Nonadiabatic Transitions. *1. Atom−Atom Collisions.* Before discussing atom−diatom collisions, let us consider the case of atom−atom collisions as a reference, where only structureless rare gas atoms are considered as the collision partners. Nonadiabatic couplings involved in these fine-structure mixings are summarized in Figure 7. In many cases, the most important coupling is the radial coupling induced by the spin−orbit interaction and it is usually localized at intermediate nuclear separations between the Hund's case (c) and (a) regions as discussed in section III.A, because the character of the molecular electronic states changes rapidly at this region. However, this radial coupling cannot be involved in the fine-structure mixing between the $^3P_1$ and $^3P_0$ states and can only be responsible for fine-structure transitions between the $^3P_1$ and $^3P_2$ states or those between the $^3P_0$ and $^3P_2$ states, as depicted in Figure 7.

The rotational coupling mixes the molecular states differing in Ω by ± 1. There is only one rotational coupling, between the a($^30^-$) and B(^{31}) states, which can cause $^3P_1 \rightarrow {}^3P_0$ transitions. The nonadiabatic transition from the A($^30^+$) to a($^30^-$) states is strictly forbidden because the reflection symmetry with respect to a *collision plane* is conserved in atom−atom collisions. In mercury−rare gas collisions, this fine-structure transition has not been observed [3] probably due to the large energy separations between the related potential curves at thermal collision energies.

In the measurements of the polarization dependence of atom−atom collisions, all trajectories with the parallel polarization of the pump laser lead to the "+" component of the B(^{31}) state or the A($^30^+$) state. Since the nonadiabatic transition from the "+" component of the B(^{31}) to the a($^30^-$) states is symmetrically forbidden as well as that from the A($^31^+$) state, we can conclude that the value of the cross section for parallel polarization must be zero, as demonstrated in the collisional fine-structure transition of Ca($^3P_1 \rightarrow {}^3P_0$) with He.[23] Strictly speaking, this is due to conservation of the e/f symmetry of the rovibronic wave functions of the collision pair, and a detailed discussion of this point was presented in theoretical calculations of Ca(4s4p $^1P_1$) + He collisions.[62,63]

2. Atom−Diatom Collisions. When the collision partners are diatomic molecules, the situation is much more complicated. In C_s symmetry, the B(^{31}) state is split into the two electronic states with A′ and A″ symmetry (the 2^3A′ and 2^3A″ states), and A($^30^+$) and a($^30^-$) states are classified as the 1^3A′ and 1^3A″ states, respectively, as indicated in Figure 1. The A′ and A″ correspond to the positive and negative reflection symmetries with respect to the *molecular plane*. There are six kinds of nuclear motions which can induce nonadiabatic transitions.[51] Two radial motions and two in-plane rotations have A′ symmetry; they can connect A′ (or A″) electronic state with A′ (A″) states. One radial motion is the relative nuclear motion and the other is the vibrational motion of the diatomic molecule. One in-plane rotation is associated with an overall rotation of the system plane, and the other is an internal rotation of the diatomic molecule within the system plane. Two out-of-plane rotations have A″ symmetry and can couple A′ electronic states with A″ states. One out-of-plane rotation is associated with the rotation of the diatomic molecule and the other is that related to the overall rotation of the triatomic system; both of them are classified as the rotation of the system plane. It is not necessary to conserve the reflection symmetry with respect to the *collision plane* during the collisions because of the rotational couplings associated with the out-of-plane rotations of the diatomic molecule.

3. Qualitative Interpretation for the Hg−N_2 and Hg−CO Collisions. There are two factors which affect the probability for nonadiabatic transitions between two molecular electronic states; one is the strength of the nonadiabatic couplings between these states and the other is the energy separation between the two molecular potential surfaces at the point where the nonadiabatic transition occurs. The experimental result for Hg−N_2 indicates that the nonadiabatic transition from the $\tilde{A}(1^3A')$ to $\tilde{a}(1^3A'')$ states is negligible, even though the energy separation of these two states is small around the inner wall of the

potentials, as depicted in Figure 1 (and see paper 2). This means that the rotational couplings associated with the out-of-plane rotations are negligibly small so that the radial couplings or rotational couplings associated with the in-plane rotation, which can couple the A″ component of the $\tilde{B}$ state with the $\tilde{a}(1^3A'')$ state, are important in the nonadiabatic transition for $Hg-N_2$. In contrast, the results for Hg−CO indicate that the rotational couplings associated with out-of-plane rotation must play an important role for the Hg−CO system.

Due to the spherical-like electronic character of N_2, the electrostatic interaction between the $Hg(6^3P_J)$ and N_2 is expected to have only small anisotropy and we can rationalize the small probability of the $\tilde{A}-\tilde{a}$ nonadiabatic transition for $Hg-N_2$, given this small anisotropy, as follows. There are two kinds of anisotropy in the electrostatic interactions. One is associated with the in-plane rotation of the diatomic molecule, which determines the anisotropy of the intermolecular potential surfaces. The other is associated with the out-of-plane rotation of the diatomic molecule with respect to the direction of the 6p orbital of Hg, and it determines the energy separation between the A′ and A″ components of the $\tilde{B}$ state.[64] There must be strong correlation between these two types of anisotropy because both of them depend strongly on the anisotropy of molecular orbitals of the diatomic molecule which can mix the atomic orbitals of Hg in the molecular region. The latter type of anisotropy is important for nonadiabatic transitions between A′ and A″ states. For $Hg-N_2$, the nonadiabatic coupling associated with the out-of-plane rotation of N_2 must be small because the character of electronic states changes slowly during the rotation of N_2 perpendicular to the system plane due to its small anisotropy.

For Hg−CO, the large contribution from the rotational coupling associated with the out-of-plane rotation probably indicates large (out-of-plane) anisotropy of the electrostatic interaction. To examine the origin of this large anisotropy for Hg−CO, we refer to an ab initio calculation by Kato et al.[65] They calculated potential surfaces of the $Hg(6^3P_J)-CO$ system and found large (in-plane) anisotropy in these molecular surfaces with respect to the rotation of CO within the system plane. In their calculation, all electronic states correlating with the $^3\Pi$ states in the Hund's case (a) limit (see Figure 7) have strong attractive surfaces when Hg approaches to the C side of CO but less attractive ones when it approaches to the O side or with a T shape. Excited molecular orbitals of these electronic states are strongly mixed with an unoccupied π^* orbital of CO, because molecular states correlating with the excited triplet state of CO lay just above those associated with the excited $Hg(6^3P_J)$. The large anisotropy of the intermolecular potentials of Hg−CO is probably due to the large anisotropy of the π^* orbital of CO; its electron density must be relatively localized around the C side of CO. Therefore, the electrostatic interaction would also have large anisotropy with respect to the out-of-plane rotation of CO.

For $Hg-N_2$, the cross section with the parallel excitation has a value being about 40% of that with the perpendicular excitation in our measurement for $Hg-N_2$ as shown in Figure 5a. It shows sharp contrast to the polarization dependence predicted for the atom−atom collisions in which the cross section for the parallel polarization must drop to zero because of the conservation of the reflection symmetry with respect to the *collision plane* during the collision as explained in the discussion for the atom−atom collision. This means that the initial memory of the reflection symmetry with respect to the *collision plane* in the space-fixed frame, which must be conserved for the atom−atom collisions, has been lost at short internuclear separations for $Hg-N_2$ where the nonadiabatic transitions take place.

IV. Summary

We have measured the polarization angle dependence of the pump laser for the fine-structure changing collisions of $Hg(6^3P_1 \rightarrow 6^3P_0)$ with N_2 and CO to observe the orbital alignment effect of excited $Hg(6^3P_1)$. We have found a large polarization dependence for the $Hg-N_2$ collisions with a preference for perpendicular polarization versus the initial collision velocity. This clearly indicates that the nonadiabatic transitions responsible for this inelastic process occur mainly via the molecular $\tilde{B}$ state and not via the $\tilde{A}$ state. In contrast, the small dependence for Hg−CO, which also favors perpendicular excitation, means that there is a significant contribution from the nonadiabatic $\tilde{A}-\tilde{a}$ transition, even though the $\tilde{B}-\tilde{a}$ transition is the main route for the fine-structure changing collisions. An explanation for this large difference between the results for the $Hg-N_2$ and Hg−CO systems has been proposed based on the anisotropy of the electrostatic interaction of the $Hg(6^3P_J)$ states and the diatomic molecule (N_2 or CO).

Acknowledgment. The present study is supported in part by the Grant-in-Aid for Scientific Research (08740438 and 09740412) from the Ministry of Education of Japan.

Appendix

The wave function of the $Hg(6^3P_1)$ state prepared by linearly polarized laser radiation is

$$|(6^3P_1)\, J = 1, M_J = 0\rangle \propto |1,1\rangle_L\, |1,-1\rangle_S - |1,-1\rangle_L\, |1,1\rangle_S \tag{A-1}$$

using LS type basis functions, $|L, M_L\rangle_L\ |S, M_S\rangle_S$, where the quntization axis is taken parallel to the direction of the electric field vector ($\mathbf{E}_{las}$) of the laser radiation. The $Hg(6^3P_1)$ state is essentially two electron system (with 6s and 6p electrons), and therefore, the electronic basis functions, $|1,1\rangle_L$ and $|1, -1\rangle_L$, can be written as[66]

$$|1,\pm1\rangle_L = |0,0\rangle_l\, |1,\pm1\rangle \tag{A-2}$$

The basis functions, $|l,m_l\rangle_l$, are electronic wave functions of the 6s or 6p electron, and are proportional to spherical harmonic functions, $Y_{l,m}(\theta,\phi)$, where θ and ϕ are polar angles of each electron with respect to the direction of $\mathbf{E}_{las}$. Since $|Y_{11}(\theta,\phi)|^2 = |Y_{1-1}(\theta,\phi)|^2 \propto \sin^2\theta$, an electronic part of the $Hg(6^3P_1)$ wave function is proportional to $|Y_{11}(\theta,\phi)|^2$ distribution. Strictly speaking, the pure LS type wave function of the $Hg(6^3P_1)$ state is mixed with that of the $Hg(6^1P_1)$ state by the spin−orbit interaction. However, the contribution from the $Hg(6^1P_1)$ state, which is propotional to $|Y_{10}(\theta,\phi)|^2$ distribution, is small, and the charge cloud of the 6p electron in the $Hg(6^3P_1)$ state is therefore almost proportional to the $|Y_{11}(\theta,\phi)|^2$ distribution.

References and Notes

(1) Mitchell, A. C. G.; Zemansky, M. W. *Resonance Radiation and Excited Atoms*; Cambridge University Press: London, 1961.
(2) King, D. L.; Setser, D. W. *Annu. Rev. Phys. Chem.* **1976**, 27, 407 and references therein.
(3) Breckenridge, W. H.; Umemoto, H. *Adv. Chem. Phys.* **1982**, *50*, 325 and references therein.
(4) Cvetanovic, R. J. *Prog. React. Kinet.* **1964**, *2*, 39.
(5) Phillips, L. F. *Acc. Chem. Res.* **1974**, *7*, 135.
(6) Campbell, J. M.; Strausz, O. P.; Gunning, H. E. *J. Am. Chem. Soc.* **1973**, *95*, 740.
(7) Horiguchi, H.; Tsuchiya, S. *Bull. Chem. Soc. Jpn.* **1977**, *50*, 1661.

(8) Okunishi, M.; Hashimoto, J.; Chiba, H.; Ohmori, K.; Ueda, K.; Sato, Y. *J. Phys. Chem.* **1999**, *103*, 1742.
(9) Duval, M.-C.; D'Azy, O. B.; Breckenridge, W. H.; Jouvet, C.; Soep, B. *J. Chem. Phys*. **1986**, *85*, 6324.
(10) Duval, M.-C.; Soep, B.; Breckenridge, W. H. *J. Phys. Chem*. **1991**, *95*, 7145.
(11) Hertel, I. V.; Schmidt, H.; Bahring, A.; Meyer, E. *Rep. Prog. Phys*. **1985**, *48*, 375.
(12) Campbell, E. E. B.; Schmidt, H.; Hertel, I. V. *Adv. Chem. Phys*. **1988**, *75*, 37.
(13) Bahring, A.; Hertel, I. V.; Meyer, E.; Schmidt, H. *Z. Phys. A* **1983**, *312*, 293.
(14) Bahring, A.; Hertel, I. V.; Meyer, E.; Meyer, W.; Spies, N.; Schmidt, H. *J. Phys. B* **1984**, *17*, 2859.
(15) Bahring, A.; Meyer, E.; Hertel, I. V.; Schmidt, H. *Z. Phys. A* **1985**, *320*, 141.
(16) Hertel, I. V.; Hofmann, H.; Rost, K. A. *J. Chem. Phys*. **1979**, *71*, 674.
(17) Reiland, W.; Jamieson, G.; Tittes, H.-U.; Hertel, I. V. *Z. Phys. A* **1982**, *307*, 51.
(18) Reiland, W.; Tittes, H.-U.; Hertel, I. V.; Bonaci −Koutecky, V.; Persico, M. *J. Chem. Phys*. **1982**, *77*, 1908.
(19) Bussert, W.; Neusch fer, D.; Leone, S. R. *J. Chem. Phys*. **1987**, *87*, 3833.
(20) Kovalenko, L. J.; Robinson, R. L.; Leone, S. R. *J. Chem. Soc., Faraday Trans. 2*, **1989**, *85*, 939.
(21) Smith, C. J.; Driessen, J. P. J.; Eno, L.; Leone, S. R. *J. Chem. Phys*. **1992**, *96*, 8212.
(22) Visticot, J.-P.; de Pujo, P.; Sublemontier, O.; Bell, A. J.; Berlande, J.; Cuvellier, J.; Gustavsson, T.; Lallement, A.; Mestdagh, J. M.; Meynadier, P.; Suits, A. G. *Phys. Rev. A* **1992**, *45*, 6371.
(23) Smith, C. J.; Spain, E. M.; Dalberth, M. J.; Leone, S. R.; Driessen, J. P. J. *J. Chem. Soc., Faraday Trans*. **1993**, *89*, 1401.
(24) Manders, M. P. I.; Ruyten, W. M.; Beucken, F. v. d.; Driessen, J. P. J.; Veugelers, W. J. T.; Kramer, P. H.; Vredenbregt, E. J. D.; van Hoek, W. B. M.; Sandker, G. J.; Beijerinck, H. C. W.; Verhaar, B. J. *J. Chem. Phys*. **1988**, *89*, 4777.
(25) Manders, M. P. I.; Driessen, J. P. J.; Beijerinck, H. C. W.; Verhaar, B. J. *Phys. Rev. A* **1988**, *37*, 3237.
(26) Rettner, C. T.; Zare, R. N. *J. Chem. Phys*. **1982**, *77*, 2416.
(27) Suits, A. G.; Hou, H.; Davis, H. F.; Lee, Y. T.; Mestdagh, J.-M. *J. Chem. Phys*. **1991**, *95*, 8178.
(28) Suits, A. G.; Hou, H.; Davis, H. F.; Lee, Y. T. *J. Chem. Phys*. **1992**, *96*, 2777.
(29) Breckenridge, W. H.; Jouvet, C.; Soep, B. *J. Chem. Phys*. **1986**, *84*, 1443.
(30) Yamanouchi, K.; Isogai, S.; Tsuchiya, S.; Duval, M.-C.; Jouvet, C.; d'Azy, O. B.; Soep, B. *J. Chem. Phys*. **1988**, *89*, 2975.
(31) Fuke, K.; Saito, T.; Nonose, S.; Kaya, K. *J. Chem. Phys*. **1987**, *86*, 4745.
(32) Duval, M. C.; Soep, B.; van Zee, R. D.; Bosma, W. B.; Zwier, T. S. *J. Chem. Phys*. **1988**, *88*, 2148.
(33) Duval, M. C.; Soep, B. *J. Phys. Chem*. **1991**, *95*, 9075.
(34) Wallace, I.; Breckenridge, W. H. *J. Chem. Phys*. **1992**, *97*, 2318.
(35) Wallace, I.; Kaup, J. G.; Breckenridge, W. H. *J. Phys. Chem*. **1991**, *95*, 8060.
(36) Soep, B.; Abb s, S.; Keller, A.; Visticot, V. *J. Chem. Phys*. **1992**, *96*, 440.
(37) Quayle, C. J. K.; Bell, I. M.; Tak cs, E.; Chen, X.; Burnett, K.; Segal, D. M. *J. Chem. Phys*. **1993**, *99*, 9608.
(38) Chen, X.; Burnett, K.; Segal, D. M. *J. Chem. Phys*. **1991**, *95*, 8124.
(39) Alford, W. J.; Burnett, K.; Cooper, J. *Phys. Rev. A* **1983**, *27*, 1310.
(40) Alford, W. J.; Andersen, N.; Burnett, K.; Cooper, J. *Phys. Rev. A* **1984**, *30*, 2366.
(41) Alford, W. J.; Andersen, N.; Belsley, M.; Cooper, J.; Warrington, D. M.; Burnett, K. *Phys. Rev. A* **1985**, *31*, 3012.
(42) Behmenburg, W.; Kroop, V.; Rebentrost, F. *J. Phys. B* **1985**, *18*, 2693.
(43) Olsgaard, D. A.; Havey, M. D.; Sieradzan, A. *Phys. Rev. A* **1991**, *43*, 6117.
(44) Burnett, K. *Phys. Rep*. **1985**, *118*, 339.
(45) Bieniek, R. J.; Julienne, P. S.; Rebentrost, F. *J. Phys. B* **1991**, *24*, 5103.
(46) Lewis, E. L.; Harris, M.; Alford, W. J.; Cooper, J.; Burnett, K *J. Phys. B* **1983**, *16*, 553.
(47) Kleiber, P. D.; Lyyra, A. M.; Sando, K. M.; Zafiropulos, V.; Stwalley, W. C. *J. Chem. Phys*. **1986**, *85*, 5493.
(48) Bililign, S.; Kleiber, P. D.; Kearney, W. R.; Sando, K. M. *J. Chem. Phys*. **1992**, *96*, 218.
(49) Wong, T. H.; Kleiber, P. D. *J. Chem. Phys*. **1995**, *102*, 6476.
(50) Lin, K. C.; Kleiber, P. D.; Wang, J. X.; Stwalley, W. C.; Leone, S. R. *J. Chem. Phys*. **1988**, *89*, 4771.
(51) Ohmori, V.; Kurosawa, T.; Chiba, H.; Okunishi, M.; Ueda, K.; Sato, Y.; Nikitin, E. E. *J. Chem. Phys*. **1995**, *102*, 7341.
(52) Ohmori, K.; Takahashi, T.; Chiba, H.; Saito, K.; Nakamura, T.; Okunishi, M.; Ueda, K.; Sato, Y. *J. Chem. Phys*. **1996**, *105*, 7464, 7474.
(53) Fujii, A.; Ebata, T.; Ito, M. *Chem. Phys. Lett*. **1989**, *161*, 93.
(54) Hines, M. A.; Michelson, H. A.; Zare, R. N. *J. Chem. Phys*. **1990**, *93*, 8557.
(55) Schüler, V. H.; Keyston, J. E. *Z. Phys*. **1931**, *72*, 423.
(56) Moore, C. E. *Atomic Energy Levels;* U.S. Government Printing Office: Washington, D. C., 1971; Vol. III.
(57) Nikitin, E. E. *J. Chem. Phys*. **1965**, *43*, 744.
(58) Grosser, J. *J. Phys. B* **1981**, *14*, 1449.
(59) Berengolts, A.; Dashevskaya, E. I.; Nikitin, E. E. *J. Phys. B* **1993**, *26*, 3847.
(60) In most of the previous reports, different kind of expressions, $\sigma(\theta) = (\sigma_{\|} + \sigma_{\perp})/2 + [(\sigma_{\|} - \sigma_{\perp})/2] \cos[2(\theta - \theta_0)]$, were usually used, but those have essentially the same functional form as the present expression in eq 2.
(61) Hirschfelder, J. O.; Curtiss, C. F.; Bird, R. B. *Molecular Theory of Gases and Liquids*; John Wiley & Sons: New York, 1963.
(62) Pouilly, B.; Alexander, M. H. *J. Chem. Phys*. **1987**, *86*, 4790.
(63) Pouilly, B.; Alexander, M. H. *Chem. Phys*. **1990**, *145*, 191.
(64) Hickman, A. P. *J. Phys. B* **1982**, *15*, 3005.
(65) Kato, S.; Jaffe, R. L.; Komornicki, A.; Morokuma, K. *J. Chem. Phys*. **1983**, *78*, 4567.
(66) In this appendix, we ignore the procedure of the antisymmetrization to simplify the problem.